Molybdate as corrosion inhibitor for hot dip galvanised steel scribed to the substrate A study based on global and localised electrochemical approaches

Coelho, L. B.; Fava, E. B.; Kooijman, A. M.; Gonzalez-Garcia, Y.; Olivier, M. G.

DOI
10.1016/j.corsci.2020.108893

Publication date
2020

Document Version
Accepted author manuscript

Published in
Corrosion Science

Molybdate as corrosion inhibitor for hot dip galvanised steel scribed to the substrate: a study based on global and localised electrochemical approaches

L.B. Coelho [a,], E.B Fava [b], A.M. Kooijman [c], Y. Gonzalez-Garcia [c], M.-G. Olivier [a,d]*

[a] Materials Science Department, Faculty of Engineering, University of Mons, 20 Place du Parc, 7000 Mons, Belgium
[b] Materials Science and Engineering Undergraduate Program, Federal University of Santa Catarina (UFSC), 88040-900 Florianópolis, SC, Brazil
[c] Department of Materials Science and Engineering, Delft University of Technology, 2628CD, Delft, The Netherlands
[d] Materia Nova asbl, Avenue Copernic 1, 7000 Mons, Belgium

ABSTRACT

The effect of sodium molybdate in inhibiting galvanic corrosion of Zn coating and mild steel is addressed. The inhibitor's performance was appraised by Zero Resistance Ammeter on HDG/mild steel galvanic coupling model in 0.05 M NaCl (+ 5 mM Na_2MoO_4) media. The effectiveness of Na_2MoO_4 was evaluated on HDG substrate mechanically scratched to reach the steel. Scanning Vibrating Electrode Technique was employed for assessing the distribution of j from scribed HDG surfaces. This local electrochemistry approach was repeated in NaCl solution to examine the behaviour of HDG when the Zn-coating is partially removed. Surface analysis supported all electrochemical results.

Keywords

A. mild steel; A. zinc; C. neutral inhibition; C. cathodic protection; C. interfaces

1. Introduction

Zinc is extensively used as a sacrificial coating in the case of the corrosion protection of steel in a wide range of applications such as automotive, building and household appliance industries. However, the degree of protection provided by the zinc layer is not uniform across the entire steel surface, as the coating is susceptible to localised attack when exposed to chloride-containing media [1]. In the last twenty years, in parallel to the progressive regulations of Cr(VI), new families of protective compounds have been tested to improve the life-span of zinc coatings with no need for thickness increase [1–5]. Nonetheless, there is still a great need to identify (or develop) corrosion inhibitors that behave efficiently when the steel substrate is locally exposed upon (electro)chemical dissolution or mechanical removal of the Zn-rich coating. Such a situation is not only encountered during application but often during transportation and storage of the material as well.

Hot-dip galvanised steel (HDG) is produced by dipping a steel sheet into a bath of molten zinc. After cooling of the zinc-coated steel strip, skin-pass rolling is usually applied to define the final coating texture. The peaks on the surface of the working rolls are pressed into the zinc strip, creating depressions covering about 50% of the original surface [6]. Skin-passed surfaces have increased roughness, which is an essential parameter for promoting more contact area for mechanical interlocking with the primer or lubricants [7]. Such surface roughening is also reported to contribute to the chemical adhesion of the primer (increased number of functional groups per unit surface area), which explains why this treatment is widely used in the automobile industry [6]. This procedure was reported to affect the corrosion properties of galvanised steels by altering the zinc surface activity in comparison to its as-coated state [7]. The skin-passed structure of HDG comprising "summits" and "valleys" can be visualized in Fig. 1 (roll marks are indicated by black arrows in Fig. 1 (b), (c) and (e)). Therefore, in this work, it was decided to preserve the skin-passed structure of industrial HDG as much as

possible; on the contrary to of studies in which the top-surface of HDG (or zinc) specimens were ground prior to corrosion testing [1,8–11].

In the first part of this article, the inhibitive effect of sodium molybdate towards a hot-dip galvanised steel/mild steel galvanic coupling model was evaluated in 0.05 M NaCl solution, using the Zero Resistance Ammeter (ZRA) technique. The model was designed to test the inhibitor performance under critical conditions – such as a defective Zn coating associated with a considerably exposed steel surface. Hence, the HDG and the steel electrodes presented an area ratio equal to 1. In this case, despite the cathodic protection of the steel provided by zinc, the intense galvanic corrosion process would lead to significant local consumption of the Zn coating. Hence, the interest is to apply environmentally-friendly corrosion inhibitors to minimise the dissolution rate of sacrificial Zn, which is particularly high in chloride-containing electrolytes. While the majority of modelling investigations used either bi-electrodes comprising pure Zn [4,12–15] or single-electrode industrial samples [1,2,12], the ZRA model considered in this work consists of HDG and mild steel electrodes presenting industrially treated surfaces.

The choice of sodium molybdate as an inhibitor was based on a preliminary screening study which indicated the high inhibition efficiency of Na_2MoO_4 towards the same HDG/mild steel galvanic coupling model here employed. Moreover, different authors have considered sodium molybdate as a non-toxic [16] or a green inhibitor [1].

After evaluating the performance of sodium molybdate through the galvanic coupling model/ZRA approach, further studies were carried out to understand its inhibition mechanism towards severely scribed HDG. The Scanning Vibrating Electrode Technique (SVET) was employed to locally monitor the anodic and cathodic activities over scribed HDG surfaces, whose underlying steel substrate was revealed, immersed in 0.05 M NaCl with or without 5 mM Na_2MoO_4. Previous investigations using the SVET carried out on galvanised steel systems,

have contributed significantly to achieving a deeper comprehension of the underlying corrosion and inhibition phenomena [12,17,18].

Furthermore, the severity of the defect (whether the underlying Fe substrate is exposed or not) on the resulting corrosion behaviour of scratched HDG in NaCl medium was also evaluated by SVET and complementary SEM-EDX analysis. Although a constant probe-to-sample distance is commonplace for SVET measurements, the experimental approach here addresses the applicability of the technique on scribed coated-systems presenting difference in height before corrosion testing.

2. Materials and methods

2.1. Hot-dip galvanised steel and mild steel samples

Industrial hot-dip galvanised steel (HDG) plates (Extragal Z100, ~0.4 mm thick, ArcelorMittal - France) were employed for both ZRA and SVET analyses. The skin-passed Zn coatings were about 15 µm thick (weight of approximately 57.5 g/m²) and comprised Al and Fe (0.36 and 0.25 wt.%, respectively). Additionally, commercial mild steel plates (cold rolled SAE 1009, ~0.5 mm thick, Masson's Steel - France) constituted the HDG/mild steel galvanic couple model for ZRA testing. This low alloyed carbon steel is typically employed in the automotive industry. All surfaces were degreased by acetone under ultrasonic cleaning, washed with distilled water and dried with compressed air before electrochemical testing [19] (mild steel coupons were also etched for 30 s in acidic solution (Ridoline C72, Henkel - Belgium) before the washing step).

2.2. Chemicals

The reference and inhibitor-containing electrolytes were the 0.05 M NaCl (pH = 6.3) [1] and the 0.05 M NaCl + 5 mM Na_2MoO_4 (pH = 6.4), respectively. All chemicals were

purchased from Alfa Aesar and presented a degree of purity of 99.9% at least. It is important to emphasize that the Na_2MoO_4 compound does not meet any of the hazard criteria established by REACH [20] nor OSHA [21] regulations.

2.3. ZRA monitoring

A HDG/mild steel galvanic coupling model was designed for ZRA testing. Rectangular coupons of both materials (2 x 7 cm^2) were protected using tape for corrosion testing (3M™ Scotchrap™ 50). Each tape strip was previously pierced with a 1.4 mm diameter punch tool, thereby generating samples with ~1.5 cm^2 of exposed area. The area ratio of the electrodes was equal to 1. A schematic representation of the HDG/mild steel galvanic coupling configuration for ZRA testing is presented in Fig. 2.

The AMETEK Parstat 2273 and the Powersuite® were used as potentiostat and programming interface, respectively. HDG coupons, mild steel coupons and an Ag/AgCl/KClsat (+197 mV/SHE) electrode were respectively employed as working, counter and reference electrodes. The 3-electrode set-up was fixed inside a home-built cell (polypropylene) by forming an equilateral triangle of ~3 cm side (placed inside a Faraday cage). Taking advantage of the fact that the electrode area ratio was equal to 1, the computed galvanic currents were converted into galvanic current density (j_{galv}) for plotting purposes.

2.4. Potentiodynamic polarisation measurements

Potentiodynamic polarisation curves were obtained for the HDG electrode (anodic branch) and the mild electrode (cathodic branch) in 0.05 M NaCl. In both cases, Plexiglass cells were fixed on the surface of 5 cm x 5 cm plates, leaving exposed areas of ~7.1 cm^2. Starting from OCP, the polarisation was conducted at a scan rate of 0.5 mV s^{-1} for anodic/cathodic

branches. Prior to testing, the OCP was followed for 30 min, and steady potentials were attained.

An Ag/AgCl/KCl_{sat} (+197 mV/SHE) was used as reference electrode and a platinum coil as auxiliary electrode. Such as for ZRA testing, experiments were performed inside a Faraday cage using the AMETEK Parstat 2273 potentiostat.

2.5. Scanning Vibrating Electrode Technique (SVET) analysis

SVET was employed to investigate localised corrosion processes over scratched HDG samples exposed to 0.05 M NaCl solution in the absence and presence of 5 mM of inhibitor (sodium molybdate).

The surfaces of the HDG specimens (cleaned as previously described) were entirely covered by protective insulating tape (3M™ Ruban Polyester 8402) except on test areas of 0.78 mm^2 (1 mm diameter window). Next, the exposed surfaces were manually scribed using a scalpel prior to testing. The resulting scratches were about 0.5±0.1 mm in length and ~12 or ~18 µm in depth (the scribing procedure is described in detail in the topic below). The defects of ~12 µm depth partially removed the Zn-rich layer without reaching the steel substrate while those with ~18 µm depth completely revealed the steel substrate. Both types of analysed scratches are schematically illustrated in Fig. 3(a).

The equipment and corresponding software were supplied by Applicable Electronics™ (AE) and Science Wares™, respectively. The current density was continuously recorded on a 41 x 41 grid (scanned area of ~1360 µm x ~1360 µm (on average), spatial resolution of ~34 µm) whose centre was placed on the centre of the exposed area of the sample. An insulated Pt-Ir probe (Microprobe™) with a Pt-black deposit (ø = ~20 µm) was used (probe-to-sample distance = 80±5 µm). The SVET system was calibrated in each working electrolyte (2 mL) following the AE system manual (resistivity values were 342 and 153 ohm.cm for the reference and molybdate-containing electrolytes, respectively). This calibration method is a common

practice among researchers working with the AE device and is described in detail elsewhere [22]. The SVET peak-to-peak voltage signal was converted to values of current flux density along the axis of probe vibration [23]; in the vertical direction (j_Z), in this case. The probe vibration frequency was 80 Hz and the peak-to-peak vibration amplitude was 40 µm. The current density was calculated as shown in Eq. 1 (j_Z is the current density in the Z-axis, ρ is the solution resistivity, ΔV is the potential gradient in the solution measured between two points at a distance Δr (vibration amplitude)).

$$j_Z = -\frac{1}{\rho}\frac{\Delta V}{\Delta r} \quad (1)$$

After a run-in immersion period of ~10 min, 4 scans of ~35 min started each 45 min, leading to a total testing time of ~180 min. All SVET measurements were repeated twice, and reproducibility was asserted (the location of anodes and cathodes varied but always corresponded to the scribe-related regions accordingly).

2.5.1. Scribing procedure and estimation of defect depths

Preliminary 3D profile analysis (VHX 5000 Keyence digital Microscope) indicated that the variability of the scribing procedure was relatively high in terms of whether the underlying mild steel substrate was reached or not. Therefore, several exposed regions (1 mm diameter window) were created on each covered HDG specimen used for SVET analysis. The exposed surfaces were either manually scribed using the scalpel (area reserved for local electrochemistry) or indented with controlled load using a microhardness testing (Vickers 110 MV1 equipment). Produced Vickers indents were either ~12 or ~18 µm depth (ISO 6507). Then, based on 3D profile analysis, the distances between the indent bottoms and their top-surfaces (~12 or ~18 µm) were used as a reference for determining the scratch depths. Thereby, only scratches presenting ~12 or ~18 µm were selected for SVET testing, and the remainder of the surface was covered by insulating tape. This method for estimation of defect depths is

schematically illustrated in Fig. 3(b). It must be stressed that, as the scribing procedure is user-dependent, this "reverse engineering" method for selecting scribes with a target depth is relatively time-consuming.

2.6. Microscopy analysis

Optical microscopy analysis was performed using the VHX 5000 Keyence Digital Microscope. Scanning Electron Microscopy coupled to an Energy Dispersive X-ray (SEM-EDX) Spectrometer analysis was employed after electrochemical testing. Before inserting samples in the Hitachi SU8020 microscope, their surfaces were rinsed with distilled water and dried with compressed air. It is important to mention that the detection limit of the employed EDX was ~0.1%.

3. Results and discussion

3.1. ZRA analysis of the HDG/mild steel galvanic coupling

Fig. 4 presents the evolution of the j_{galv} and E_{galv} curves recorded for 180 min in 0.05 M NaCl in the absence and presence of sodium molybdate. First, an apparent increase of E_{galv}, from ~-940 mV to ~-870 mV Vs Ag/AgCl, was depicted when molybdate was present in the electrolyte (anodic inhibitor [1]). More importantly, the change in potential was accompanied by a considerable decrease of j_{galv} passing, on average (triplicate tests), from 20.9±2.3 to 11.4±1.9 µA/cm². These results highlighted the beneficial effect of Na_2MoO_4 on the galvanic corrosion of the galvanised steel/mild steel pair.

It was interesting to note that while the obtained E_{galv} values were quite steady and reproducible, the j_{galv} curves presented a lower reproducibility and a spikier behaviour. This behaviour was related to the dynamic nature of this galvanic coupling, and different factors might have contributed to it, namely: bulk precipitation of corrosion products temporarily

covering the active surfaces; progressive consumption of a heterogenous Zn-rich layer (from its top surface down to the Al-Fe intermetallic phases at the interface with the substrate); and the eventual exposition of the steel substrate (of HDG) upon local dissolution of the Zn coating, introducing micro-cathodes on the (mainly) anodic HDG electrode. As galvanised steel electrode was barely polarised when galvanically coupled to mild steel (as revealed by potentiodynamic polarization analysis (Fig. 5)), small variations in E_{galv} could lead to significant variation in j_{galv}.

The resulting HDG surfaces after ZRA experiments performed in 0.05 M NaCl or 0.05 M NaCl + 5 mM Na_2MoO_4 solutions were compared through optical and scanning microscopy analyses (Fig. 1). First, the surface changes induced by corrosion testing were observed in the circular exposed areas delimited by protective tape (Fig. 1(a) and (d)). Secondly, in both cases, the "summits" of the skin-passed structured remained rather unaltered, and the "valleys" were preferentially affected (Fig. 1(b) and (e)). Nonetheless, while these depressions seemed corroded after immersion in NaCl solution (Fig. 1(b)), they appeared extensively covered by precipitates upon exposure to molybdates (Fig. 1(e)). As a reference, a HDG surface before corrosion testing is also displayed (Fig. 1(c)).

To further investigate these surface modifications, SEM-EDX analyses were performed on both surfaces (Fig. 6 and Fig. 7). After testing in the NaCl reference solution, the HDG surface appeared considerably attacked, as illustrated in the secondary electron image presented in Fig. 6(a). From the corresponding EDX elemental maps obtained from the same location, it was confirmed that corrosion took place in a localised manner. From a defect of about ~50 µm of diameter is was possible to apprehend that corrosion of the Zn-rich layers was intense enough to reach the underlying steel substrate (Fig. 6(c)). Many authors consider the Zn layer so is susceptible to pitting corrosion in Cl^- solution [3,17,24]: partial hydrolysis of Zn^{2+} could induce localised acidification and drive pitting propagation [11,25]. The signals of Al were also higher

at this location (Fig. 6(d)), which was reflective of Al-Fe intermetallic phases mainly present at the coating-substrate interface [26].

Moreover, the presence of corrosion products was preferentially assigned in association with the Fe-rich regions from HDG (Fig. 6(e, f)). It is important to note, however, that only a limited amount of precipitates was detected on the corroded HDG surface - which accorded well with preliminary optical microscope analysis (results not displayed). In fact, during galvanised steel/mild steel galvanic corrosion, the hydrolysis of zinc ions controls the pH slightly below a neutral value [12,14,15,27] (Eq. 2 and Eq. 3) and Zn hydroxides are soluble under near-neutral conditions (up to pH ~8) [8,28].

$$Zn^{2+} + H_2O \rightarrow ZnOH^+ + H^+ \quad (2)$$

$$ZnOH^+ + H_2O \rightarrow Zn(OH)_{2(aq)} + H^+ \quad (3)$$

Although the exposed steel regions on the HDG substrate most likely acted as local cathodes, white corrosion products of Zn were barely detected, indicating that developed pH was not high enough to allow stable precipitation [12,14,29,30]. According to different works on zinc/steel galvanic coupling [15,27], sufficient high pH enabling the development of $Zn(OH)_2$ (Eq. 4) occurs solely on regions of the steel relatively distant from the anolyte emerging from zinc. As addressed in the following sections, the high intensity of chloride ions on the localised attacked areas (Fig. 6(f)) also resonates a limited local alkalinisation effect.

$$Zn^{2+} + 2OH^- \rightarrow Zn(OH)_{2(s)} \quad (4)$$

Concerning the mild steel electrode ~3 cm distant from the HDG (Fig. 2), it was uncorroded until completion of the test, which asserted the cathodic protection effect. Local EDX analysis could not detect Zn on the remote mild steel surface (Fig. 6(g)). As a result of the considerably high mild steel/HDG area ratio and intense alkalinisation of the catholyte [14,15,31], the Zn^{2+} cations probably reacted with OH^- ions relatively far from the cathode (Eq. 4) [13,30], likely resulting in bulk precipitation of $Zn(OH)_2$ [27].

On the other hand, in the presence of molybdates, the SEM-EDX analysis showed that the HDG surface was significantly protected, without visible traces of corrosion (Fig. 7). Instead, the presence of a fine Mo/O-rich phase was identified. The intensity of molybdate precipitation was not equal across the surface, as further precipitation seemed to have occurred on the recesses of the skin-passed topography (Fig. 1(e)). It might be the case that the "valleys" of the roughened surface acted as a site for more intense anodes than the "summit" regions, due to their more intense local oxygen-depletion conditions. Considering molybdate as an anodic inhibitor (Fig. 4), the formation of the Mo-based precipitates would preferentially occur on these anodic regions. More importantly, the apex of the Zn surface remained quite protected. Furthermore, the signals related to Fe and Al were homogeneously distributed throughout the surface, suggesting no localised corrosion attack (Fig. 7); contrary to that observed in the absence of inhibitor (Fig. 6). The detection of Fe and Al signals did not necessarily mean that the Zn-rich layers dissolved, as the X-radiation has a micrometric penetration depth in the matter. Finally, it is worth noting that Mo was not detected on the surface of the mild steel counter electrode (EDX spectra not presented).

These results pointed out the formation of a protective molybdate-containing film. In neutral aqueous molybdate solution, MoO_4^{-2} ions condense into heptamolybdate polyanion ($[Mo_7O_{24}]^{-6}$), Eq. 5 [1]), which is particularly voluminous and able to protect Zn surfaces [32]. The polymolybdate ion can adsorb onto the positively charged surface of HDG, resulting in protection towards chloride penetration [32]. This mechanism helps to illustrate why the molybdate film appeared in the electrode preferentially working as an anode (HDG) (Eqs. 2 and 3) and not in the cathodic one (mild steel).

$$7[MoO_4]^{-2} + 8H^+ \leftrightarrow [Mo_7O_{24}]^{-6} + 4H_2O \quad (5)$$

Although the ZRA/model method constituted a valuable tool for asserting the effectiveness of the inhibitor, a local electrochemical technique approach was envisaged for

evaluating its performance towards more realistic configurations. Therefore, for the proceeding work, corrosion activities related to scratched HDG surfaces were monitored by SVET in the presence (and absence) of sodium molybdate.

3.2. SVET analysis on scratched HDG

3.2.1. 0.05 M NaCl – evaluation of defects

First, HDG samples presenting ~12 µm-depth defects (partial removal of the Zn-rich layers) were tested. Fig. 8 shows SVET maps obtained between 10-45 min and 145-180 min of immersion in 0.05 M NaCl solution. The scratch was located at x equal to ~600 µm and y between ~550 and ~950 µm. The SVET plots present the time-dependent distribution of current density (µA/cm²), with anodic and cathodic activities displayed in red and blue, respectively.

Evident cathodic activity (oxygen reduction reaction [11,15,17,27,33]) could be perceived on the Zn coating around the defect while anodic activity was depicted directly over the Zn-rich defect area. The lack of cathodic activity on the defect area was expected, as the steel substrate was not supposed to be revealed in this case. However, the fact that the scratch played the role of the anode during the entire test duration (~180 min) was somewhat surprising for two reasons: first, as the entire exposed surface was Zn-rich, a random-like distribution of anodes/cathodes was expected; secondly, the appearance of cathodic activity related to the steel substrate was expected to occur during the testing period (based on the outcomes from the 3 h-ZRA tests), as a consequence of the thinned Zn layer in the defect region. Scribing the outer layer of the HDG sample removed the oxide layer present on the industrial galvanised steel surface [30]. Thereby, the generated defective surface preferentially acted as an anode while the non-scribed, surrounding Zn-rich surface, constituted the cathode of the galvanic pair. It should likewise be noted that the scribe would be oxygen-deficient and would, therefore, more

likely act as an anode. Also employing SVET, Montemor et al. [33] observed exclusive anodic activity over scratches produced on HDG/sol-gel coating systems.

The distribution configuration of anodic/cathodic cells remained similar throughout the test. An evident decrease in the magnitude of both anodic and cathodic reactions was registered from the first to the last scan (Fig. 8(a) and(b)). As the intensity of the cathodic current density also decreased, the suppression of anodic activity could not be only related to changes over time of the probe-to-sample distance upon dissolution of the anodes [27]. The achieved current density values were similar to those presented by Taryba et al. [2] working on defective primer-coated HDG using SVET-SIET.

The scratched and corroded HDG surface was examined employing SEM-EDX after the SVET tests. The backscattered electron image displayed in Fig. 9(a) highlights evident precipitation of white corrosion products around the scratch, in concentric rings centred on the defect - as often observed for cut-edge HDG systems [34]. The location of these products (region limited by dashed lines in Fig. 8(c)) mainly corresponded to the frontier between regions presenting anodic and cathodic activity (Fig. 8(a) and (b)). Similar frontier regions exhibiting intense precipitation of products and absence of activity have been reported [2]. The minor occurrence of white corrosion products directly over the anodic sites is supported by Salgueiro et al. observations [35]: precipitation requires a sufficiently intense associated cathodic process. Furthermore, partial hydrolysis of Zn^{2+} prevents the anolyte pH from increasing (Eqs. 2 and 3) [14,15,30,36], resulting in conditions not alkaline enough to promote precipitation of $Zn(OH)_2$ [13,14].

The observed attenuation in the electrochemical activities (Fig. 8(b)) could be related to the precipitation of a protective film which progressively placed anodic and cathodic sites further apart from each other. According to Taryba et al. [2], the locations of formation of whitish corrosion products match with areas presenting decreased cathodic current density. In

the present case also, the precipitation and associated current decrease (Fig. 8(b)) occurred on a region which had presented cathodic activity at the beginning of immersion (region limited by the dashed lines, Fig. 8(a)). The protective nature of zinc (hydr)oxides is a matter of debate and it certainly depends on the local pH and chemistry conditions [3,8,9,11,15,30]. Nonetheless, different authors [12,27,35] have reported the formation of a thin and dense protective film of zinc oxide on cathodic sites distant from an active Zn surface. For instance, the barrier effect of Zn coatings is also often credited to the formation of stable corrosion products [30,35,37].

Concerning the elemental maps presented in Fig. 9 from (b) to (f), a few points should be addressed. First, proper EDX signals could not be detected from the upper side of the scratch. This artefact (indicated by a circle in Fig. 9(b)) was related to the topographic features combined with the position of the X-radiation detector. Except for this relatively inaccessible portion of the defect, the EDX signals arising from the other regions could be appropriately detected. Secondly, the precipitates located far from the scribed surface (concentric rings) most likely constituted Zn (hydr)oxides (corresponding high intensities of Zn and O signals).

It was interesting to note that the Zn signal remained particularly high almost on the entire surface of the scratch. This was a confirmation that the underlying substrate was indeed not revealed upon scribing in this case. The only exception was the region on the left side of the scratch, which presented particularly low Zn signals and corresponding high intensities of Fe and Al (Fig. 9 (c) and (d)). This site was coincident to the centre of anodic activity depicted in the SVET maps (Fig. 8). As evidenced in the elemental maps, the anodic attack also partially encompassed a nearby region outside the defect region (the darkened region in Fig. 9(a)). The anodic activity which started on the scribed surface most likely triggered a further dissolution of Zn on neighbouring zones due to slight acidification effect induced by hydrolysis [15,31]. Corrosion products based on Cl other than O also appeared as stable phases on the focal points of anodic attack. Furthermore, the particularly high Cl concentration on these areas (Fig. 9(f))

accords well with the pit-like defects that reached the steel substrate of the Zn coating from the HDG/mild steel pair (Fig. 6(f)). Indeed, several authors have reported the precipitation of Cl-containing corrosion products over anodic spots on zinc surfaces [2,33,38]. For example, simonkolleite ($Zn_5(OH)_8Cl_2$) is usually stable in a pH range between 6 and 8 [11,34,39] (Eq. 6 [12]).

$$4Zn(OH)_{2(aq)} + Zn^{2+} + 2Cl^- \rightarrow Zn_5(OH)_8Cl_{2(s)} \quad (6)$$

A modelling study on the galvanic coupling of zinc/steel pointed out to the correlation of Zn and Cl distribution on the steel surface [30]. Hence, the progressive exposition of steel – and the corresponding increase of the area supporting oxygen reduction reaction (ORR) - might also have contributed to the enhanced local concentration of Cl on defective spots (Eq. 7) [35,38] – such as previously observed in (Fig. 6(f)). Although the exposed steel had certainly supported cathodic reactions, the overall electrochemical activity on this location remained anodic, as measured by SVET.

$$4Zn(OH)_{2(aq)} + 5Zn^{2+} + 8OH^- + 2Cl^- \rightarrow Zn_5(OH)_8Cl_{2(s)} \quad (7)$$

Despite insoluble hydroxychlorides being often associated with passivity breakdown [10], a few investigations have paid attention to their potential ability to protect zinc [3,40]. Although the formation of thin and dense zinc (hydr)oxides might indeed explain the decrease of corrosion rate depicted over time by SVET, the local precipitation of $Zn_5(OH)_8Cl_2$ could also have played a role. Finally, as illustrated in Fig. 9, the progressive exposition of Al/Fe intermetallic phases present at the coating/substrate interface might also have contributed: the kinetics of corrosion on Al-rich intermetallics or on Fe–Zn alloy layer are clearly lower than on zinc coating or on steel [41,42]. The exact reason for the decrease of corrosion activity remains unclear to date and further analyses will be envisaged in the future.

Fig. 10 shows SVET maps obtained in 0.05 M NaCl solution from a HDG sample whose introduced scratch (~18 µm-depth, located at x equal to ~550 µm and y between ~300 and ~900

μm) exposed the steel substrate. Contrarily to the previous case, here, an evident cathodic activity could be directly detected over the scratch, from the first (10-45 min) to the last (145-180 min) obtained SVET maps (Fig. 10(a) and (b), respectively). The anodic activity mainly developed on the surrounding outer surface, over non-scribed Zn-rich layers. In this case, the sacrificial role of scratched galvanised steel was undoubtedly demonstrated: anodic activity on the Zn coating and ORR on steel (Eq. 8 and Eq. 9, respectively) [8,9,14,33]. The distribution of anodic/cathodic activity remained practically unaltered over time. However, the intensity of the anodic reaction presented a pronounced increase, indicating the progressive dissolution of Zn in the regions external to the defect.

$$Zn \rightarrow Zn^{2+} + 2e^{-} \quad (8)$$

$$O_2 + 2H_2O + 4e^{-} \rightarrow 4OH^{-} \quad (9)$$

By comparing the total currents obtained from integrating SVET current densities [43] for both types of scribed surfaces (Fig. 11), it could be seen that, in the first half of the tests, the anodic activity was higher for the partially removed Zn layer. Nonetheless, as a function of time, the anodic currents presented opposing trends: the total anodic activity remained increasing for the completely scribed Zn coating, while it showed a pronounced decrease for the partially scribed one, finally reaching lower, steady values. This trend could be explained by the following reasons: in the first case, anodic activities on the external surfaces around the cathodic defect would be entirely detected, driven by the continuous exposition of the substrate; whereas in the second case, the anodic dissolution of Zn in the defect area would progressively occur in deeper (or more hidden) regions of the defect, hampering the detection by the SVET probe.

On the other hand, the total cathodic currents from both scribed surfaces were relatively similar and remained relatively constant throughout the tests. This outcome seemed unexpected, as the rate of ORR, which limits the rate of the anodic reaction of Zn, was expected to be higher

on steel than on zinc [8,44]. Nevertheless, one should consider that the cathode/anode area ratio for the exposed steel sample was much lower than for the partially scribed coating. Indeed, in the latter case, a larger area of intact zinc coating was demonstrated to support reduction reactions (Fig. 8). Moreover, by considering the same reasoning as for the anodic currents, the cathodic activities would most likely be underestimated for the completely scribed Zn layer, as the probe would miss part of the activity occurring on the steel substrate.

The quantitative comparison of current densities between samples presenting clearly distinct configurations (resulting in a distinct distribution of anodic and cathodic sites) is often a difficult task. In the present cases, meaningful activities from the corrosion processes would occur at a certain distance (down to ~12 or ~18 µm) below the defined surfaces of analysis.

Although the ideal condition of constant scan height sought for SVET analysis is often undermined due to surface evolution processes inherent to corrosion, the major drawback of the scribing approach here proposed is that the difference in height of the scribed region/intact surface would be higher than any disparity in height resulting from the *in-situ* dissolution of anodes during SVET testing. Nonetheless, different investigations [45–50] have made use of SVET for studying scribed coated systems of various nature/thicknesses, particularly for self-healing purposes [2,51,52]. Accurate quantification of this artefact would be hardly obtained, and, in the authors' knowledge, no attempts have been made in this direction. An alternative and more accurate way for measuring local galvanic current densities would be to mount sections of the HDG and mild steel surfaces side-by-side, ensuring electrical connection from the back. Meanwhile, the capability of scanning at a constant height over rough surfaces, with the probe following the surface topography is an emerging technology [53].

The SEM-EDX investigation (Fig. 12) revealed that much higher amounts of corrosion products were generated for this HDG sample presenting a deeper scratch. Moreover, intense Fe signals were assigned to the entire scribed surface (except on the upper side of the scratch

subjected to detection artefacts) and to the surrounding external regions as well (Fig. 12(c)). The final distribution of corrosion products was similar to the two-region pattern often observed for cut-edge corrosion [15,27,31], in which visible white precipitates only partially cover the more active (anodic) zones. According to different studies that addressed the distribution of corrosion products and corresponding pH stability ranges, precipitation of Zn cations as insoluble species [13,31] often occurs at intermediate pH zones between the increased OH^- and Zn^{2+} concentrations produced by the cathodic and anodic reactions, respectively.

The coincident depletion of Zn and enrichment in Fe (Fig. 12(b) and (d), respectively) confirmed the hypothesis of increased Zn dissolution nearby the cathodic defect. The direct exposition of the steel substrate seemed responsible for the enhanced corrosion products precipitation over and around the defect. The composition of these compounds was mainly based on Zn, O and Cl, as indicated by the respective elemental maps.

Here clearly, the corrosion products formed could not attenuate corrosion rates over time (Fig. 10(a) and (b)). The white precipitates comprised loose/flocculent particles that were not effective in covering the surface (Fig. 12(a)) [17,27,36]. In the case of cut-edge corrosion, Zn products have been considered either as protective [17] or as non-protective phases [14]. Anyway, the alkalinity produced in the present case was expected to be lower than in the case of HDG cut-edge, as a result of the considerably higher cathode/anode area ratio of the latter [12,17,27,31,34,38,54].

3.2.2. Severely scribed HDG in 0.05 M NaCl + 5 mM Na_2MoO_4

Sodium molybdate performed as a promising inhibitor on a HDG/steel model designed to mimic a scratched HDG sample whose steel substrate would become exposed entirely. The effectiveness of the inhibitor towards severely scribed HDG surfaces was investigated through the same SVET/SEM-EDX approach employed in the reference solution. Fig. 13 presents the SVET maps obtained from a scratched HDG surface (~18 µm-depth defect, located at x equal

to ~600 µm and y between ~400 and ~1000 µm) exposed to 0.05 M NaCl + 5 mM Na_2MoO_4 electrolyte between 10-45, 100-135 and 145-180 min.

At the beginning of immersion, only minor cathodic activity emerged from the scratch region (Fig. 13(a)). Next, as shown in Fig. 13(b), the cathodic response from the same location became relatively more pronounced, while an anodic process with low intensity spread out around the defect. By the end of the test (Fig. 13(c)), a larger area seemed to support cathodic activity, and anodic reactions appeared more concentrated closer to the scratched zone.

The time-resolved inhibition effect of molybdate was highlighted from 4 consecutive SVET scans. Line profiles of current density were constructed crossing the active surfaces exposed to 0.05 M NaCl or 0.05 M NaCl + 5 mM Na_2MoO_4 (Fig. 14). The directions of the line profiles (respectively indicated by the lines r-r' and i-i' in the SVET maps for the reference (Fig. 10) and inhibitive media (Fig. 13)) were chosen to maximise the information of the collected j_Z. The magnitudes of j_Z related to the cathodic defects were quite similar in both cases, but considerably more spatially confined in the molybdate electrolyte. Furthermore, the intensities of anodic j_Z from the Zn-rich outer surfaces were visibly higher in the NaCl than in the NaCl + Na_2MoO_4 solution, over the entire testing duration.

Although Mo-rich films are claimed to be stable in pH values up to 12 [32], some works mentioned that reduced molybdate species tend to redissolve in solution [3,55]. In comparison to the results achieved on severely scribed HDG in 0.05 M NaCl solution (Fig. 10), molybdate species were shown to considerably decrease the corrosion process – either in terms of intensity of the anodic/cathodic j or in terms of extension of the active areas. Contrary to the present case, in the reference medium, SVET had not detected anodic activity occurring on the intact Zn-coating regions immediately close to the defect (Fig. 10). In that case, the extensive corrosion products build-up nearby the scratch (Fig. 12) probably shifted the anodic spots to farther

locations – which reflected the increased anodic activity depicted over time on the periphery of the precipitation process (Fig. 10(b)).

Fig. 15 presents a SEM image (and corresponding elemental maps) of the resulting HDG surface after exposure to the NaCl/Na_2MoO_4 electrolyte. According to the secondary electron image (Fig. 15(a)), the galvanised steel seemed considerably protected, including both scribed and non-scribed regions. The Fe signal appeared particularly intense over the scratch, testifying the mechanical removal of the Zn-rich layers (Fig. 15(b)). In addition, precipitate layers appeared associated with the defect region. These products consisted of a molybdate-based film, as the associated locations were depleted in Zn and enriched in O and Mo (Figs. 15 (b), (e) and (f), respectively). The distribution of the O and Mo signals was closely related to each other. By taking Eq. 5 into account, some acidity is needed for the formation of the molybdate polyanion; which might be a reason for the preferential precipitation of the protective layer directly over the spots of the Zn surface subjected to anodic dissolution. Most importantly, the molybdate was able to prevent the process of local dissolution of Zn from the regions neighbouring the scratch – as opposed to that observed in the inhibitor-free medium (Fig. 12(b)).

The presence of Cl was not detected on the exposed surface, suggesting the protective behaviour of the molybdate film concerning chloride-induced corrosion attack (and eventual formation of insoluble zinc chloride hydroxides). The mismatch between the distributions of Fe and O is also worth mentioning: this fact suggested that dissolution of the steel substrate did not take place. This is an essential point because inhibitive species of Zn might eventually extinguish its sacrificial character and in turn, drive corrosion of steel [2,17]. Nevertheless, the patchy and heterogeneous character of the molybdate film was not ideal for extended protection [4] – which might explain the increase of corrosion activities eventually depicted after 3 h of immersion (Fig. 13(c)).

4. Conclusions

This work highlighted the promising performance of sodium molybdate as a corrosion inhibitor of hot-dip galvanised steel presenting a severely scribed surface (steel substrate exposed) immersed in 0.05 M NaCl. The industrial surface state (skin-passed) of the HDG plates was maintained for all testing specimens.

The effectiveness of Na_2MoO_4 was attested on a HDG/mild steel model constructed to simulate a pessimistic galvanic coupling scenario (1:1 cathode/anode area ratio). This scenario was an unfavourable relative to HDG scribed to the substrate, in which the exposed cathode would be much smaller than the anode. By employing ZRA and SEM-EDX analysis, the compound was demonstrated to behave as an anodic inhibitor for HDG coupled to mild steel, preventing the localised attack of the Zn coating.

The effectiveness of the molybdate salt was investigated towards a configuration close to galvanic corrosion conditions typically encountered in practice for HDG, namely on a defective Zn coating presenting a scratch revealing the steel substrate. Based on SVET analysis, the inhibitor was shown to considerably decrease (up to 3 h) the intensity and extension of the anodic/cathodic activities related to the external Zn-rich layers/exposed steel surface. A molybdate-rich film was detected onto anodic sites located on the Zn-rich areas surrounding the scratch, limiting the dissolution of Zn on these peripheral regions.

This study also showed that the severity of the defect is a critical factor on the resulting corrosion behaviour of the HDG system, as the underlying steel substrate might be revealed or not. In case of partial removal of the Zn coating, a local anodic attack appeared associated with the scratched region, while the cathodic activity spread around the defect. Conversely, this situation was reversed when the steel substrate was completely exposed: the cathodic reaction was mainly assigned to the defect region while the anodic reaction was depicted on the external Zn-rich surface. The fact that the scan height was not constant for the scribed surfaces was a

drawback of the localised approach here described. Nonetheless, the use of SVET is still a powerful approach for investigating scribed coated systems whose coating/substrate present clearly different electrochemical responses.

Acknowledgements

The author L.B. Coelho acknowledges the Research Institute of Materials Science and Engineering of the University of Mons for financial support; the funding provided by the project TRANSPORT (Interreg France-Wallonie-Vlaanderen); the CRM-Group for providing hot-dip galvanised steel samples; the Materials Engineering Undergraduate Program from UFSC for the internship of Mr Enrico Fava performed at UMONS; and the COST action MP1407 for awarding the grant for a scientific mission with TU Delft.

Declarations of interest: none

Data availability: data will be made available on request

References

[1] I.A. Kartsonakis, S.G. Stanciu, A.A. Matei, R. Hristu, A. Karantonis, C.A. Charitidis, A comparative study of corrosion inhibitors on hot-dip galvanized steel, Corros. Sci. 112 (2016) 289–307. doi:10.1016/j.corsci.2016.07.030.

[2] M. Taryba, S.V. Lamaka, D. Snihirova, M.G.S. Ferreira, M.F. Montemor, W.K. Wijting, S. Toews, G. Grundmeier, The combined use of scanning vibrating electrode technique and micro-potentiometry to assess the self-repair processes in defects on “smart” coatings applied to galvanized steel, Electrochim. Acta. 56 (2011) 4475–4488. doi:10.1016/j.electacta.2011.02.048.

[3] S. Thomas, N. Birbilis, M.S. Venkatraman, I.S. Cole, Self-repairing oxides to protect

zinc: Review, discussion and prospects, Corros. Sci. 69 (2013) 11–22. doi:10.1016/j.corsci.2013.01.011.

[4] S.H. Zhang, G. Kong, J.T. Lu, C.S. Che, L.Y. Liu, Growth behavior of lanthanum conversion coating on hot-dip galvanized steel, Surf. Coatings Technol. 259 (2014) 654–659. doi:10.1016/j.surfcoat.2014.10.017.

[5] R.B. Figueira, C.J.R. Silva, E. V. Pereira, Hybrid sol-gel coatings for corrosion protection of hot-dip galvanized steel in alkaline medium, Surf. Coatings Technol. 265 (2015) 191–204. doi:10.1016/j.surfcoat.2015.01.034.

[6] J. Cai, J. Li, Q. Chao, E. Pavlina, P. Hodgson, Grain Size and Texture Study of Controlled Skin-Passed Hot-Dip Galvanized Coating, in: Adv. High Strength Steel Press Hardening, WORLD SCIENTIFIC, 2016: pp. 256–260. doi:10.1142/9789813140622_0043.

[7] P. Puomi, H.M. Fagerholm, J.B. Rosenholm, R. Sipilä, Effect of skin pass rolling on the primer adhesion and corrosion resistance of hot-dip galvanized (HDG) steel, J. Adhes. Sci. Technol. 14 (2000) 583–600. doi:10.1163/156856100742753.

[8] S. Thomas, I.S. Cole, Y. Gonzalez-Garcia, M. Chen, M. Musameh, J.M.C. Mol, H. Terryn, N. Birbilis, Oxygen consumption upon electrochemically polarised zinc, J. Appl. Electrochem. 44 (2014) 747–757. doi:10.1007/s10800-014-0684-0.

[9] S. Thomas, I.S. Cole, M. Sridhar, N. Birbilis, Electrochimica Acta Revisiting zinc passivation in alkaline solutions, Electrochim. Acta. 97 (2013) 192–201. doi:10.1016/j.electacta.2013.03.008.

[10] K. Aramaki, The inhibition effects of cation inhibitors on corrosion of zinc in aerated 0.5 M NaCl, Corros. Sci. 43 (2001) 1573–1588. doi:10.1016/S0010-938X(00)00144-X.

[11] S. Thomas, N. Birbilis, M.S. Venkatraman, I.S. Cole, Corrosion of zinc as a function of pH, Corrosion. 68 (2012) 1–9. doi:10.5006/1.3676630.

[12] F. Thébault, B. Vuillemin, R. Oltra, C. Allely, K. Ogle, Protective mechanisms occurring on zinc coated steel cut-edges in immersion conditions, Electrochim. Acta. 56 (2011) 8347–8357. doi:10.1016/j.electacta.2011.07.016.

[13] E. Tada, H. Kaneko, Optical visualization of concentration field of Zn2+ during galvanic corrosion of a Zn/steel couple, Corros. Sci. 52 (2010) 3421–3427. doi:10.1016/j.corsci.2010.06.014.

[14] A.G. Marques, M.G. Taryba, A.S. Panão, S. V. Lamaka, A.M. Simões, Application of scanning electrode techniques for the evaluation of iron-zinc corrosion in nearly neutral chloride solutions, Corros. Sci. 104 (2016) 123–131. doi:10.1016/j.corsci.2015.12.002.

[15] E. Tada, K. Sugawara, H. Kaneko, Distribution of pH during galvanic corrosion of a Zn/steel couple, Electrochim. Acta. 49 (2004) 1019–1026. doi:10.1016/j.electacta.2003.10.012.

[16] H. Verbruggen, H. Terryn, I. De Graeve, Inhibitor evaluation in different simulated concrete pore solution for the protection of steel rebars, Constr. Build. Mater. 124 (2016) 887–896. doi:10.1016/j.conbuildmat.2016.07.115.

[17] A.M. Simões, J. Torres, R. Picciochi, J.C.S. Fernandes, Corrosion inhibition at galvanized steel cut edges by phosphate pigments, Electrochim. Acta. 54 (2009) 3857–3865. doi:10.1016/j.electacta.2009.01.065.

[18] D.A. Worsley, S.M. Powell, H.N. McMurray, Influence of Remote Cathodes on Corrosion Mechanism at Exposed Cut Edges in Organically Coated Galvanized Steels, CORROSION. 56 (2000) 492–500. doi:10.5006/1.3280553.

[19] M. Sánchez, M.C. Alonso, P. Cecílio, M.F. Montemor, C. Andrade, Electrochemical and analytical assessment of galvanized steel reinforcement pre-treated with Ce and la salts under alkaline media, Cem. Concr. Compos. 28 (2006) 256–266. doi:10.1016/j.cemconcomp.2006.01.004.

[20] REACH, Substances restricted under REACH, (2019). https://echa.europa.eu/substances-restricted-under-reach (accessed October 16, 2017).

[21] SAFETY DATA SHEET, (2018). https://www.fishersci.com/store/msds?partNumber=AAA1922236&productDescription=sodium-molybdenum-oxide-dihydrate-&vendorId=VN00024248&keyword=true&countryCode=US&language=en.

[22] D. Snihirova, S.V. Lamaka, Y. Gonzalez-Garcia, A. Yilmaz, N. Scharnagl, M.F. Montemor, M.L. Zheludkevich, Influence of inhibitor adsorption on readings of microelectrode during SVET measurements, Electrochim. Acta. 322 (2019) 134761. doi:10.1016/j.electacta.2019.134761.

[23] G. Williams, H.A.L. Dafydd, R. Grace, The localised corrosion of Mg alloy AZ31 in chloride containingelectrolyte studied by a scanning vibrating electrode technique, Electrochim. Acta. 109 (2013) 489–501. doi:10.1016/j.electacta.2013.07.134.

[24] A.C. Bastos, M.G.S. Ferreira, A.M. Simões, Comparative electrochemical studies of zinc chromate and zinc phosphate as corrosion inhibitors for zinc, Prog. Org. Coatings. 52 (2005) 339–350. doi:10.1016/j.porgcoat.2004.09.009.

[25] J.R. Galvele, Transport Processes and the Mechanism of Pitting of Metals, J. Electrochem. Soc. 123 (1976) 464. doi:10.1149/1.2132857.

[26] S. Feliu, V. Barranco, XPS study of the surface chemistry of conventional hot-dip galvanised pure Zn, galvanneal and Zn-Al alloy coatings on steel, Acta Mater. 51 (2003) 5413–5424. doi:10.1016/S1359-6454(03)00408-7.

[27] F. Thébault, B. Vuillemin, R. Oltra, K. Ogle, C. Allely, Investigation of self-healing mechanism on galvanized steels cut edges by coupling SVET and numerical modeling, Electrochim. Acta. 53 (2008) 5226–5234. doi:10.1016/j.electacta.2008.02.066.

[28] B. Beverskog, I. Puigdomenech, Revised pourbaix diagrams for zinc at 25–300 °C,

Corros. Sci. 39 (1997) 107–114. doi:10.1016/S0010-938X(97)89246-3.

[29] L.B. Coelho, M. Taryba, M. Alves, M.F. Montemor, M. Olivier, Unveiling the effect of the electrodes area on the corrosion mechanism of a graphite - AA2024-T3 galvanic couple by localised electrochemistry, Electrochim. Acta. 277 (2018) 9–19. doi:10.1016/j.electacta.2018.04.187.

[30] A.P. Yadav, H. Katayama, K. Noda, H. Masuda, A. Nishikata, T. Tsuru, Surface potential distribution over a zinc/steel galvanic couple corroding under thin layer of electrolyte, Electrochim. Acta. 52 (2007) 3121–3129. doi:10.1016/j.electacta.2006.09.061.

[31] K. Ogle, V. Baudu, L. Garrigues, X. Philippe, Localized Electrochemical Methods Applied to Cut Edge Corrosion, J. Electrochem. Soc. 147 (2000) 3654. doi:10.1149/1.1393954.

[32] V. Shkirskiy, P. Keil, H. Hintze-Bruening, F. Leroux, T. Stimpfling, D. Dragoe, K. Ogle, P. Volovitch, MoO42− as a soluble inhibitor for Zn in neutral and alkaline solutions, Corros. Sci. 99 (2015) 31–41. doi:10.1016/j.corsci.2015.05.005.

[33] M.F. Montemor, M.G.S. Ferreira, Cerium salt activated nanoparticles as fillers for silane films: Evaluation of the corrosion inhibition performance on galvanised steel substrates, Electrochim. Acta. 52 (2007) 6976–6987. doi:10.1016/j.electacta.2007.05.022.

[34] A. Alvarez-Pampliega, K. Van Den Bergh, J. De Strycker, T. Segato, M.P. Delplancke-Ogletree, H. Terryn, Corrosion product identification at the cut edge of aluminum-rich metal-coated steel, Mater. Corros. 65 (2014) 383–391. doi:10.1002/maco.201307560.

[35] M. Salgueiro Azevedo, C. Allély, K. Ogle, P. Volovitch, Corrosion mechanisms of Zn(Mg,Al) coated steel: The effect of HCO3-and NH4+ions on the intrinsic reactivity of the coating, Electrochim. Acta. 153 (2015) 159–169. doi:10.1016/j.electacta.2014.09.140.

[36] D.D. Macdonald, Characterization of the Passive State on Zinc, J. Electrochem. Soc. 145 (2006) 3141. doi:10.1149/1.1838777.

[37] A.P. Yadav, A. Nishikata, T. Tsuru, Electrochemical impedance study on galvanized steel corrosion under cyclic wet-dry conditions-influence of time of wetness, Corros. Sci. 46 (2004) 169–181. doi:10.1016/S0010-938X(03)00130-6.

[38] A. Alvarez-Pampliega, M.G. Taryba, K. Van Den Bergh, J. De Strycker, S. V. Lamaka, H. Terryn, Study of local Na+ and Cl- distributions during the cut-edge corrosion of aluminum rich metal-coated steel by scanning vibrating electrode and micro-potentiometric techniques, Electrochim. Acta. 102 (2013) 319–327. doi:10.1016/j.electacta.2013.03.186.

[39] B. l. Lin, J. tang Lu, G. Kong, Synergistic corrosion protection for galvanized steel by phosphating and sodium silicate post-sealing, Surf. Coatings Technol. 202 (2008) 1831–1838. doi:10.1016/j.surfcoat.2007.08.001.

[40] P. Volovitch, C. Allely, K. Ogle, Understanding corrosion via corrosion product characterization: I. Case study of the role of Mg alloying in Zn-Mg coating on steel, Corros. Sci. 51 (2009) 1251–1262. doi:10.1016/j.corsci.2009.03.005.

[41] A.P. Yadav, H. Katayama, K. Noda, H. Masuda, A. Nishikata, T. Tsuru, Effect of Fe–Zn alloy layer on the corrosion resistance of galvanized steel in chloride containing environments, Corros. Sci. 49 (2007) 3716–3731. doi:10.1016/j.corsci.2007.03.039.

[42] E. Palma, J.M. Puente, M. Morcillo, The atmospheric corrosion mechanism of 55%Al-Zn coating on steel, Corros. Sci. 40 (1998) 61–68. doi:10.1016/S0010-938X(97)00112-1.

[43] G. Williams, H. Neil McMurray, Localized Corrosion of Magnesium in Chloride-Containing Electrolyte Studied by a Scanning Vibrating Electrode Technique, J. Electrochem. Soc. 155 (2008) C340. doi:10.1149/1.2918900.

[44] M. Sankar, I.S. Cole, B. Emmanuel, Electrochimica Acta Model for corrosion of metals covered with thin electrolyte layers : Pseudo-steady state diffusion of oxygen, Electrochim. Acta. 56 (2011) 7171–7179. doi:10.1016/j.electacta.2011.05.009.

[45] Y. González-García, J.M.C. Mol, T. Muselle, I. De Graeve, G. Van Assche, G. Scheltjens, B. Van Mele, H. Terryn, A combined mechanical, microscopic and local electrochemical evaluation of self-healing properties of shape-memory polyurethane coatings, Electrochim. Acta. 56 (2011) 9619–9626. doi:10.1016/j.electacta.2011.03.081.

[46] L.C. Córdoba, A. Marques, M. Taryba, T. Coradin, F. Montemor, Hybrid coatings with collagen and chitosan for improved bioactivity of Mg alloys, Surf. Coatings Technol. 341 (2018) 103–113. doi:10.1016/j.surfcoat.2017.08.062.

[47] G. Williams, R. Grace, Chloride-induced filiform corrosion of organic-coated magnesium, Electrochim. Acta. 56 (2011) 1894–1903. doi:10.1016/j.electacta.2010.09.005.

[48] A. Kakaroglou, M. Domini, I. De Graeve, Encapsulation and incorporation of sodium molybdate in polyurethane coatings and study of its corrosion inhibition on mild steel, Surf. Coatings Technol. 303 (2016) 330–341. doi:10.1016/j.surfcoat.2016.02.007.

[49] M. Yan, V.J. Gelling, B.R. Hinderliter, D. Battocchi, D.E. Tallman, G.P. Bierwagen, SVET method for characterizing anti-corrosion performance of metal-rich coatings, Corros. Sci. 52 (2010) 2636–2642. doi:10.1016/j.corsci.2010.04.012.

[50] X.F. Zhang, R.J. Chen, Y.H. Liu, J.M. Hu, Electrochemically generated sol-gel films as inhibitor containers of superhydrophobic surfaces for the active corrosion protection of metals, J. Mater. Chem. A. 4 (2015) 649–656. doi:10.1039/c5ta07443f.

[51] M.F. Montemor, D. V. Snihirova, M.G. Taryba, S. V. Lamaka, I.A. Kartsonakis, A.C. Balaskas, G.C. Kordas, J. Tedim, A. Kuznetsova, M.L. Zheludkevich, M.G.S. Ferreira, Evaluation of self-healing ability in protective coatings modified with combinations of

layered double hydroxides and cerium molibdate nanocontainers filled with corrosion inhibitors, Electrochim. Acta. 60 (2012) 31–40. doi:10.1016/j.electacta.2011.10.078.

[52] I. Recloux, Y. Gonzalez-Garcia, M.E. Druart, F. Khelifa, P. Dubois, J.M.C. Mol, M.G. Olivier, Active and passive protection of AA2024-T3 by a hybrid inhibitor doped mesoporous sol-gel and top coating system, Surf. Coatings Technol. 303 (2016) 352–361. doi:10.1016/j.surfcoat.2015.11.002.

[53] S. Kallip, T. Oppe, E. Levoll, O. Opper, K. Tiisma, T. Vinter, 3D resolved topographical SVET for localized corrosion observation, in: EUROCORR 2019, Seville, Spain, n.d.

[54] A.C. Vieira, L.A. Rocha, N. Papageorgiou, S. Mischler, Mechanical and electrochemical deterioration mechanisms in the tribocorrosion of Al alloys in NaCl and in NaNO 3 solutions, Corros. Sci. 54 (2012) 26–35. doi:10.1016/j.corsci.2011.08.041.

[55] C.G. da Silva, I.C.P. Margarit-Mattos, O.R. Mattos, H. Perrot, B. Tribollet, V. Vivier, The molybdate–zinc conversion process, Corros. Sci. 51 (2009) 151–158. doi:10.1016/j.corsci.2008.10.019.

Figures

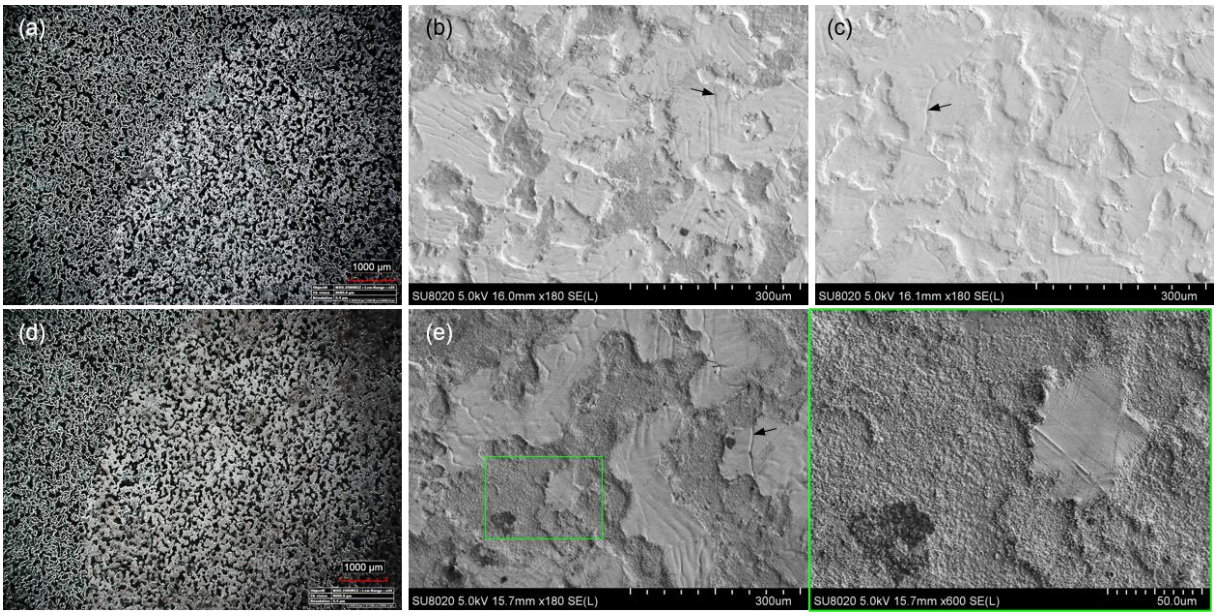

Fig. 1. (a, d) Optical and (b, e) Scanning Microscopy (secondary electron) analyses of galvanised steel surfaces from the HDG/mild steel galvanic pair after ZRA testing in (a, b) 0.05 M NaCl or in (d, e) 0.05 M NaCl + 5 mM Na_2MoO_4. (c) SEM image from a reference HDG surface. The white arrows in (b), (c) and (e) indicate roll marks from the skin-passing treatment. Inset in (e) shows a zoom of a region covered by Mo-based precipitates.

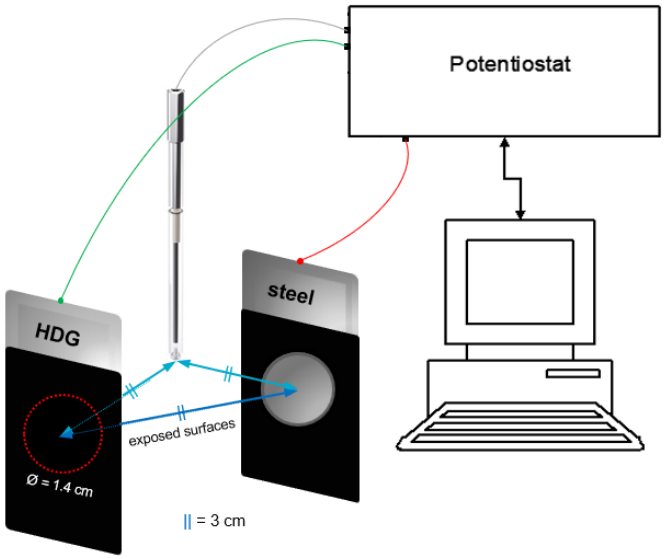

Fig. 2. Schematic representation of the HDG/mild steel galvanic coupling configuration for ZRA testing. The area ratio of the exposed surfaces (~1.5 cm²) was equal to 1.

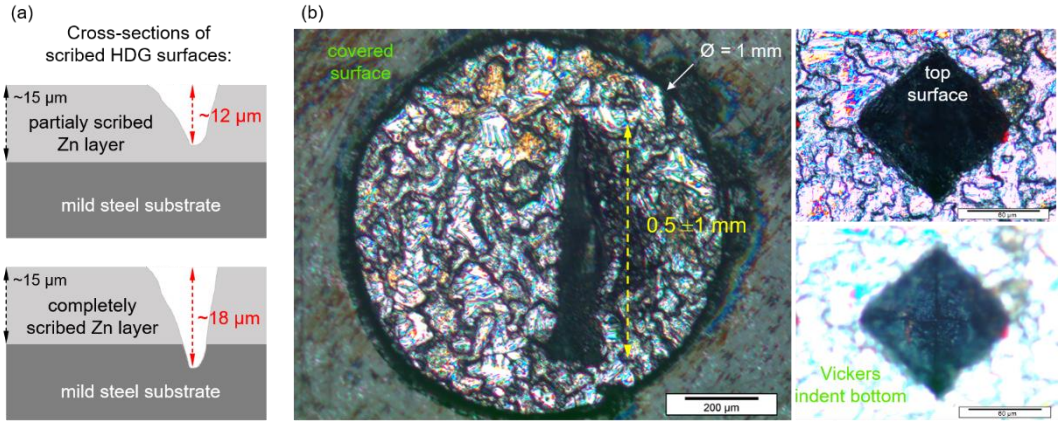

Fig. 3. (a) schematic illustration of the two types of scribed HDG surfaces analysed by SVET: scratches with ~12 or ~18 µm in depth (partial or complete removal of the Zn-rich layers, respectively) (b) schematic representation of the optical microscopy method employed for estimating defect depths: the distances between Vickers indent bottoms and their top-surfaces (~12 or ~18 µm) were used as references for selecting scratches with ~12 or ~18 µm in depth.

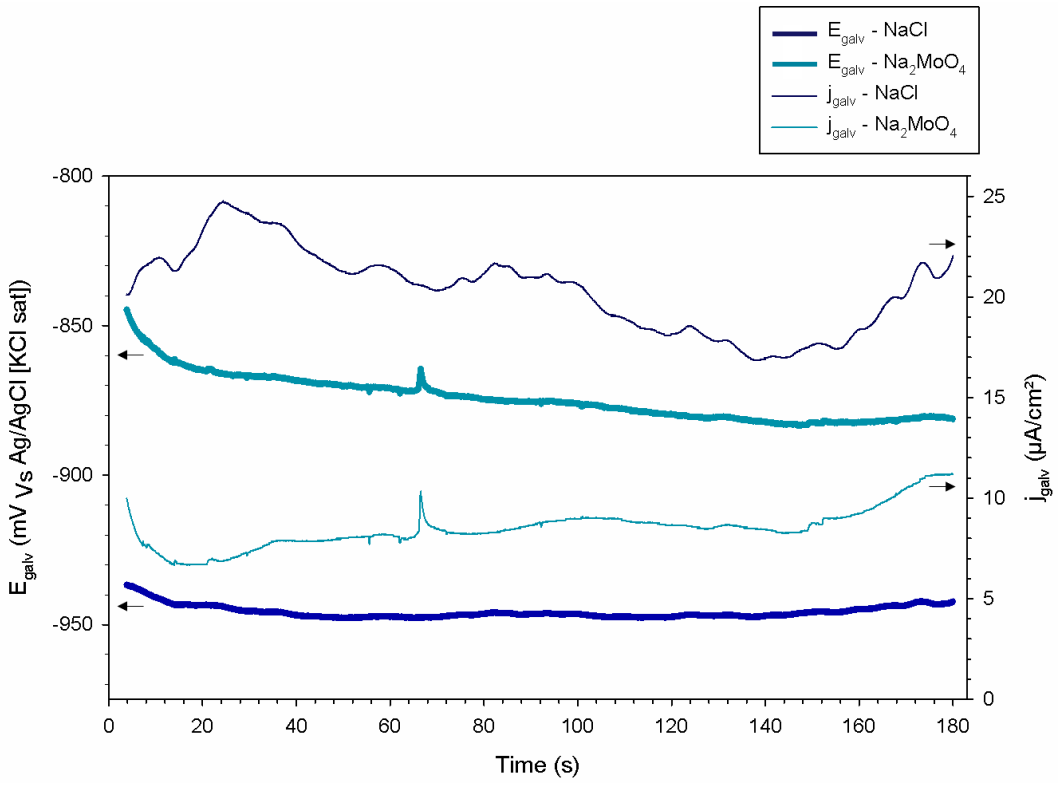

Fig. 4. ZRA curves (E_{galv} and j_{galv} evolutions) obtained from the HDG/mild steel model during 180 min of exposure in 0.05 M NaCl solution with and without 5 mM Na_2MoO_4.

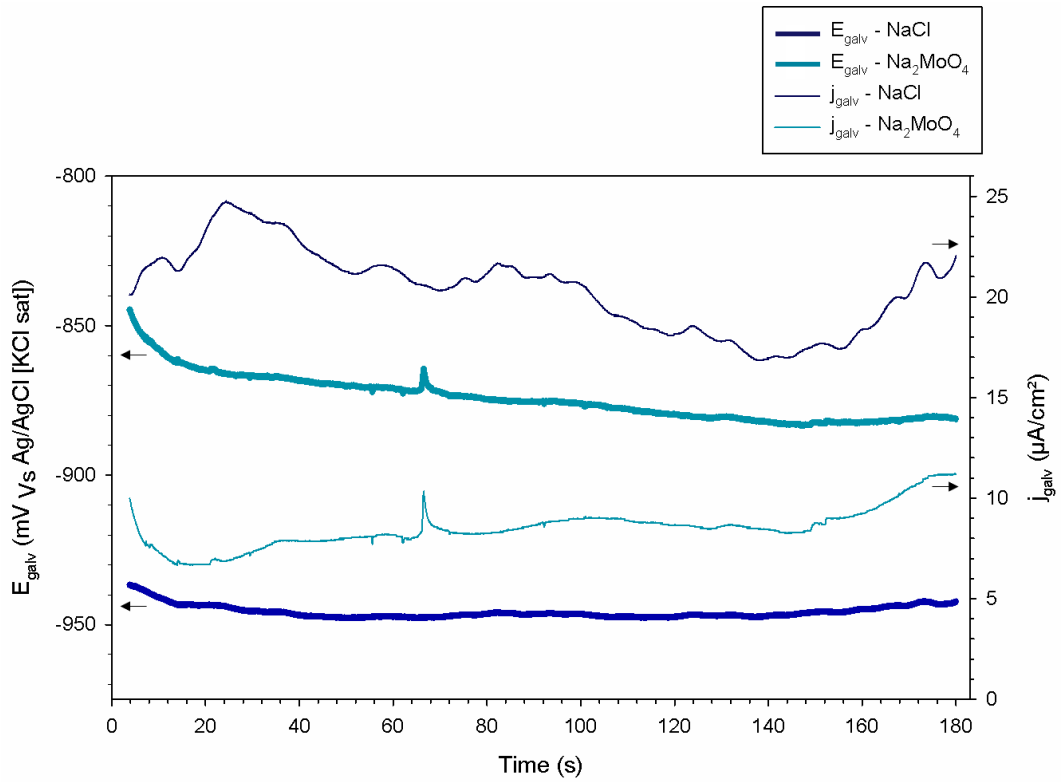

Fig. 5. Potentiodynamic polarisation curves obtained from mild steel (cathodic branch) and HDG (anodic branch) in 0.05 M NaCl solution.

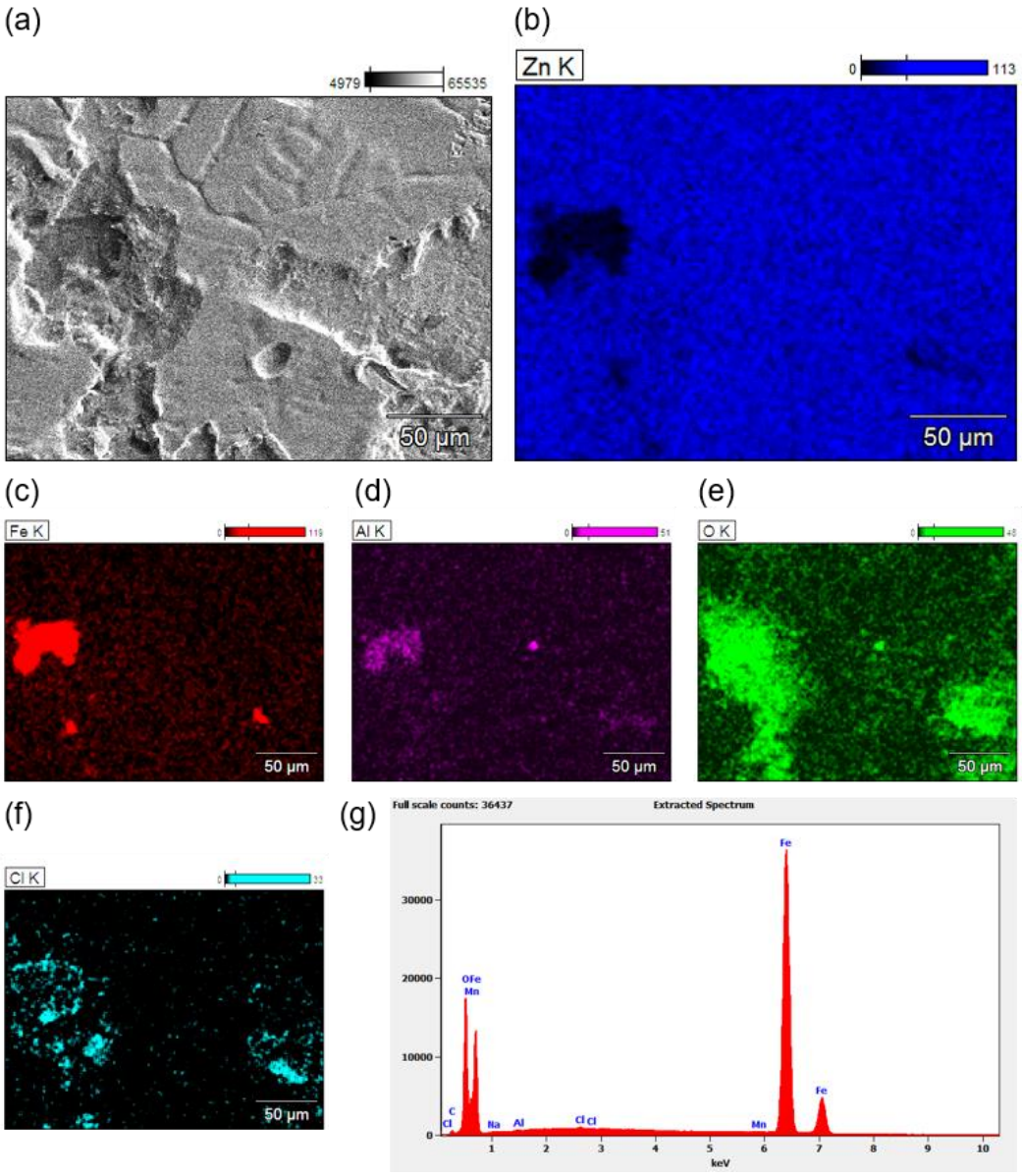

Fig. 6. SEM-EDX analysis of the galvanised steel surface from the HDG/mild steel galvanic pair after ZRA testing (180 min of immersion in 0.05 M NaCl electrolyte). (a) Secondary electron image. (b, c, d, e, f) Corresponding EDX elemental maps of Zn, Fe, Al, O and Cl. (g) Local EDX analysis of the mild steel electrode from the model after galvanic corrosion test.

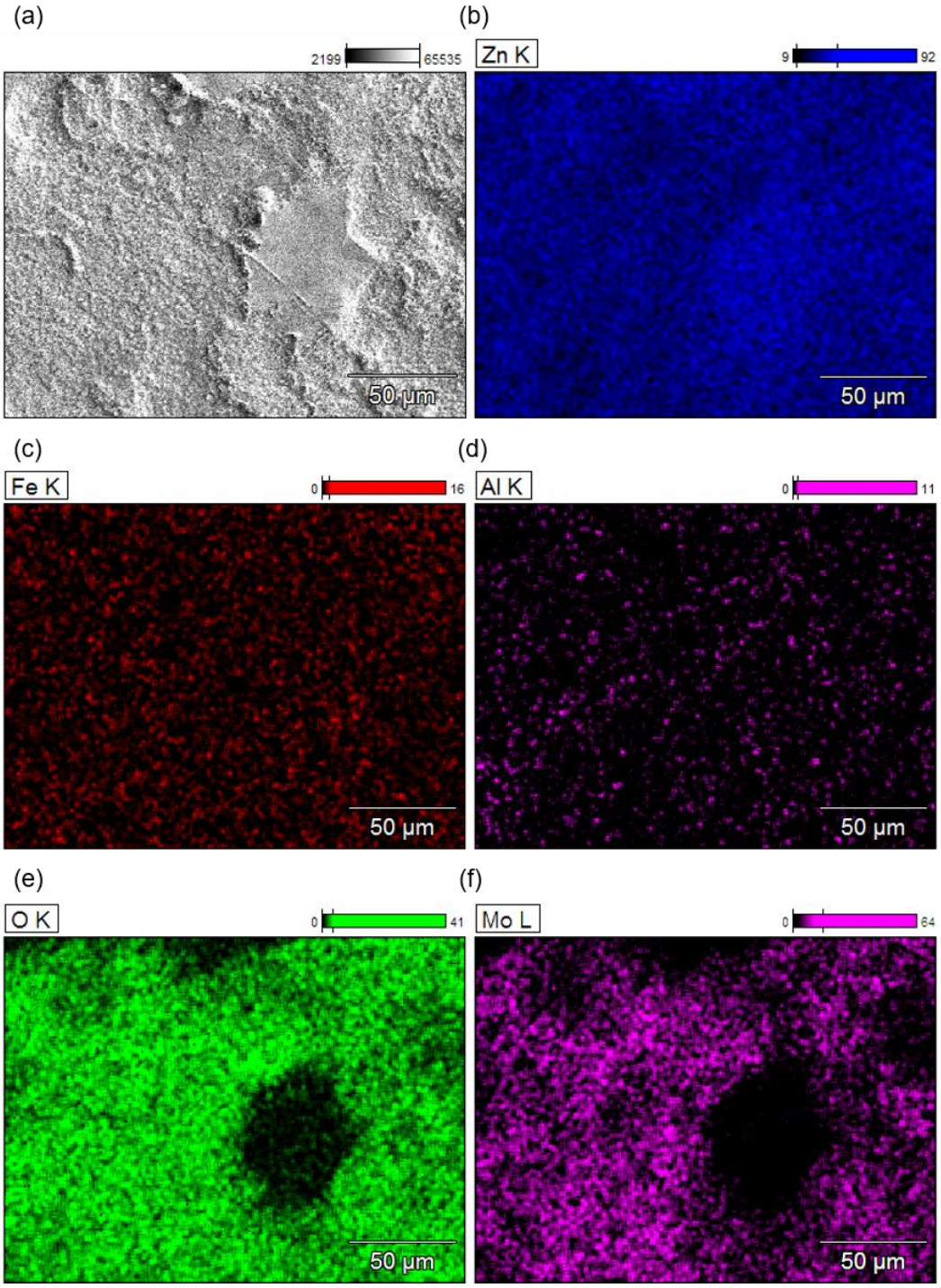

Fig. 7. SEM-EDX analysis of the HDG surface from galvanic couple model after ZRA testing (180 min of immersion in 0.05 M NaCl + 5 mM Na_2MoO_4 electrolyte). (a) Secondary electron image. (b, c, d, e, f) Corresponding EDX elemental maps of Zn, Fe, Al, O and Mo.

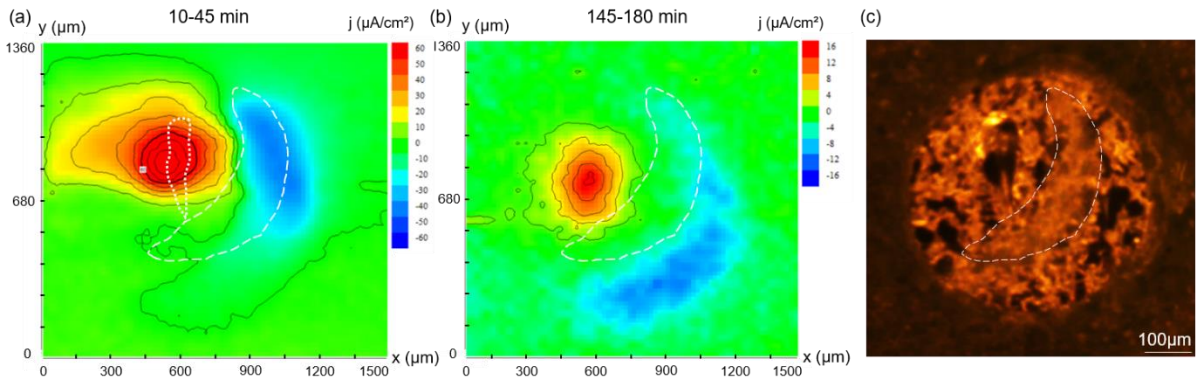

Fig. 8. Current density (µA/cm²) maps obtained by SVET from HDG presenting a partially scribed Zn coating exposed to 0.05 M NaCl solution. Scans were obtained between (a) 10-45 min and (b) 145-180 min of immersion. The scratched zone is represented by white dots in (a). (c) the corresponding optical micrograph taken after 180 min. The dashed lines in (a), (b) and (c) delimit the region with intense precipitation of white corrosion products.

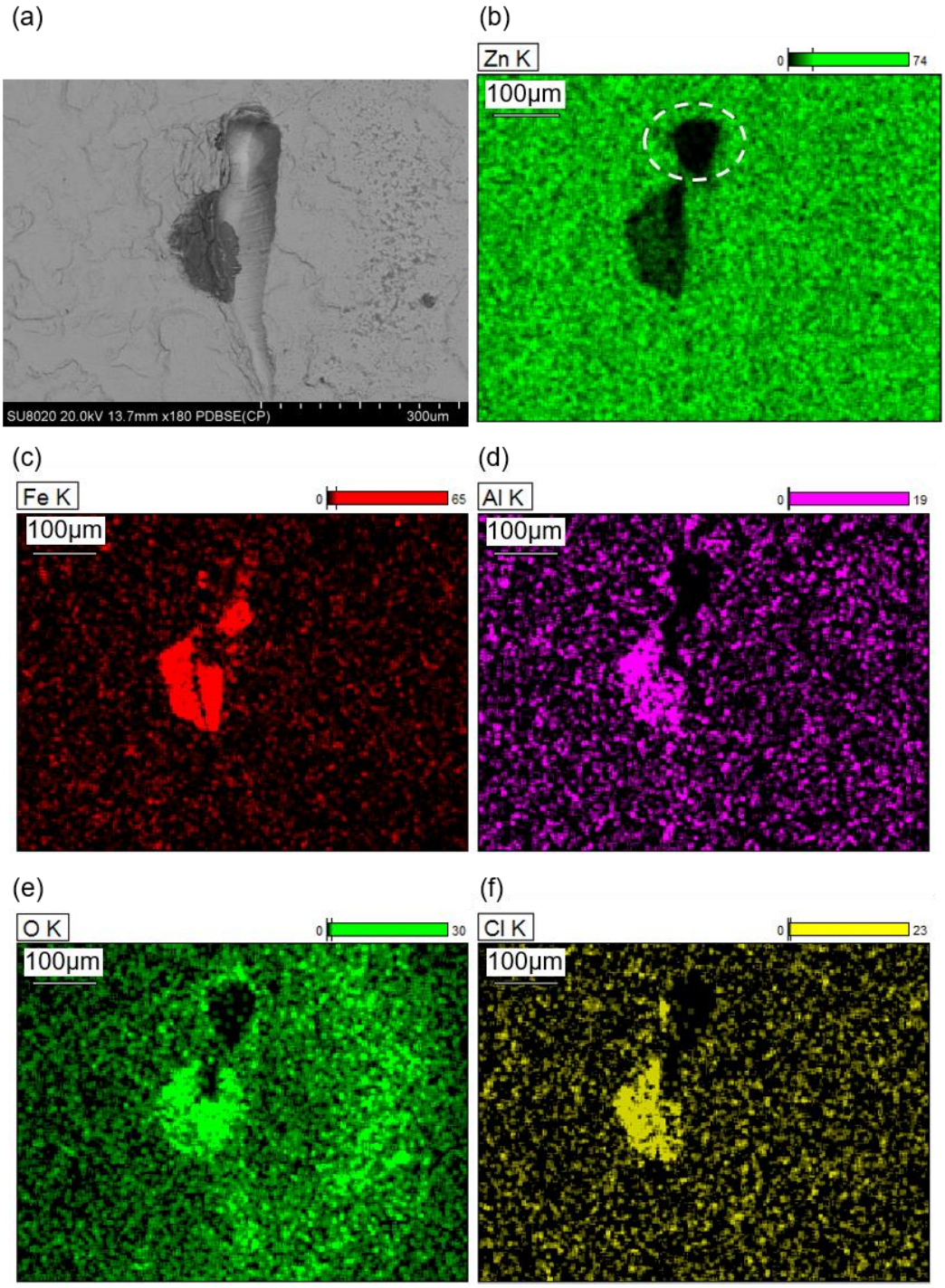

Fig. 9. SEM-EDX analysis of the moderately scribed HDG surface (~12 µm-defect depth) after 180 min of immersion in 0.05 M NaCl electrolyte. (a) Backscattered electron image electron image. (b, c, d, e, f) Corresponding EDX elemental maps of Zn, Fe, Al, O and Cl.

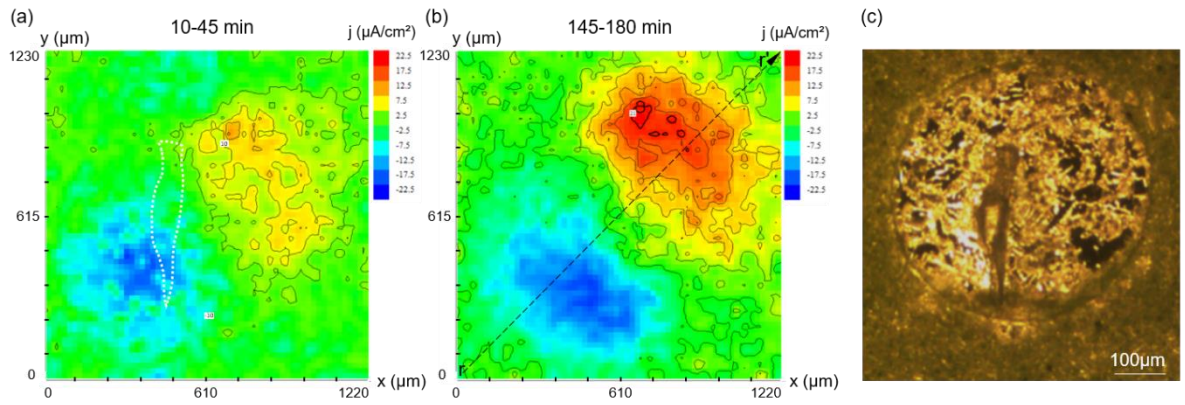

Fig. 10. Current density (µA/cm²) maps obtained by SVET from HDG presenting a completely scribed Zn coating (~18 µm-depth defect) exposed to 0.05 M NaCl solution. Scans were obtained between (a) 10-45 min and (b) 145-180 min of immersion. (c) corresponding optical micrograph taken after 180 min. The scratched zone is represented by white dots in (a). The r-r' line in (b) indicates the direction used for constructing j_Z line profiles.

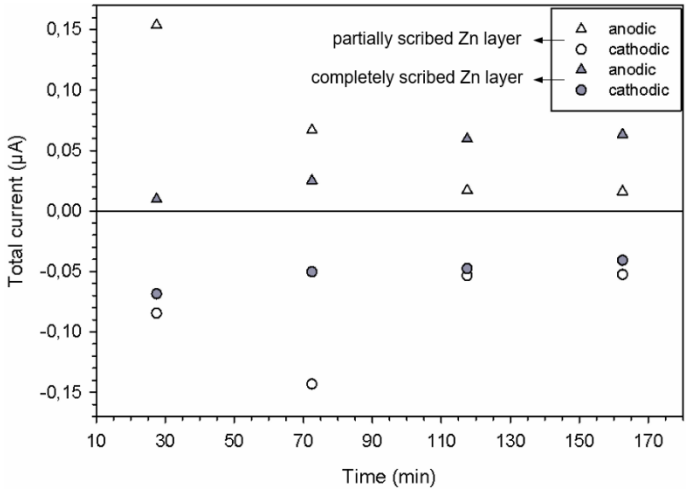

Fig. 11. Total currents obtained from integrating SVET current densities for both types of scribed HDG surfaces (partial or complete removal of Zn-rich layers) tested in 0.05 M NaCl for 180 min.

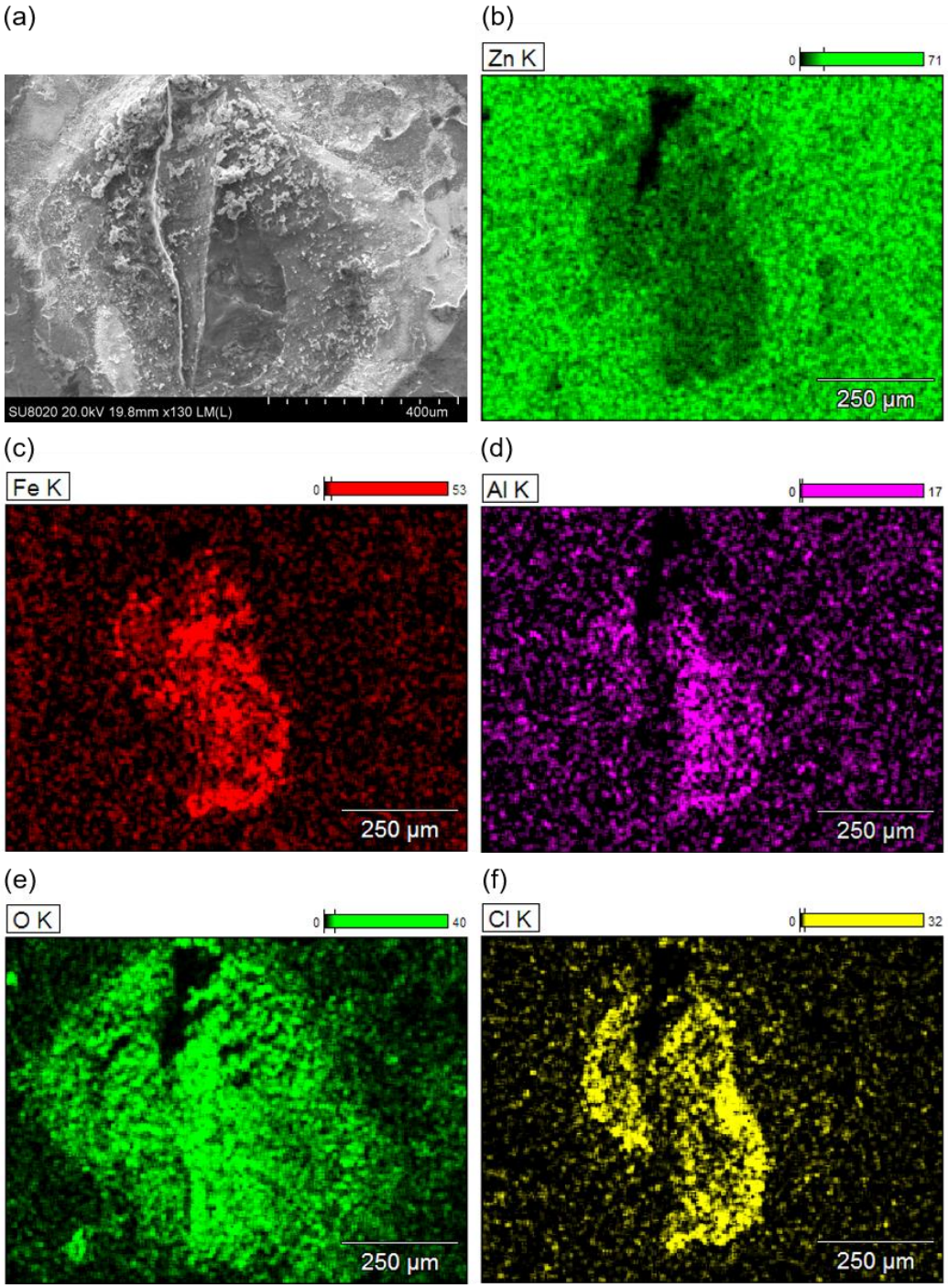

Fig. 12. SEM-EDX analysis of the severely scribed HDG surface after 180 min of immersion in 0.05 M NaCl electrolyte. (a) Secondary electron image. (b, c, d, e, f) Corresponding EDX elemental maps of Zn, Fe, Al, O and Cl.

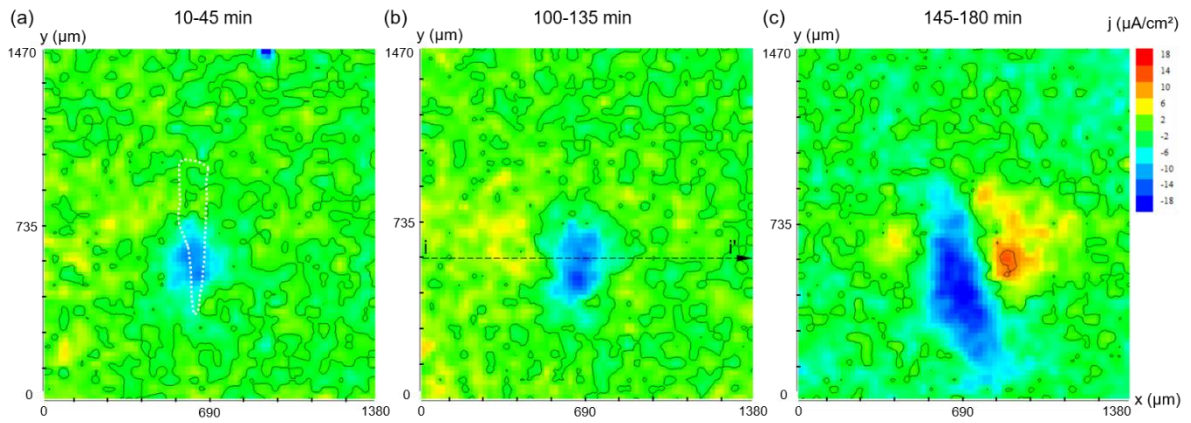

Fig. 13. Current density (µA/cm²) maps obtained by SVET on severely scratched HDG (~18 µm-depth defect) exposed to 0.05 M NaCl + 5 mM Na_2MoO_4 solution after (a) 10-45 min, (b) 100-135 min and (c) 145-180 min of immersion. The j scale is the same for all maps. The scratched zone is represented by white dots in (a). The i-i' line in (b) indicates the direction used for constructing j_Z line profiles.

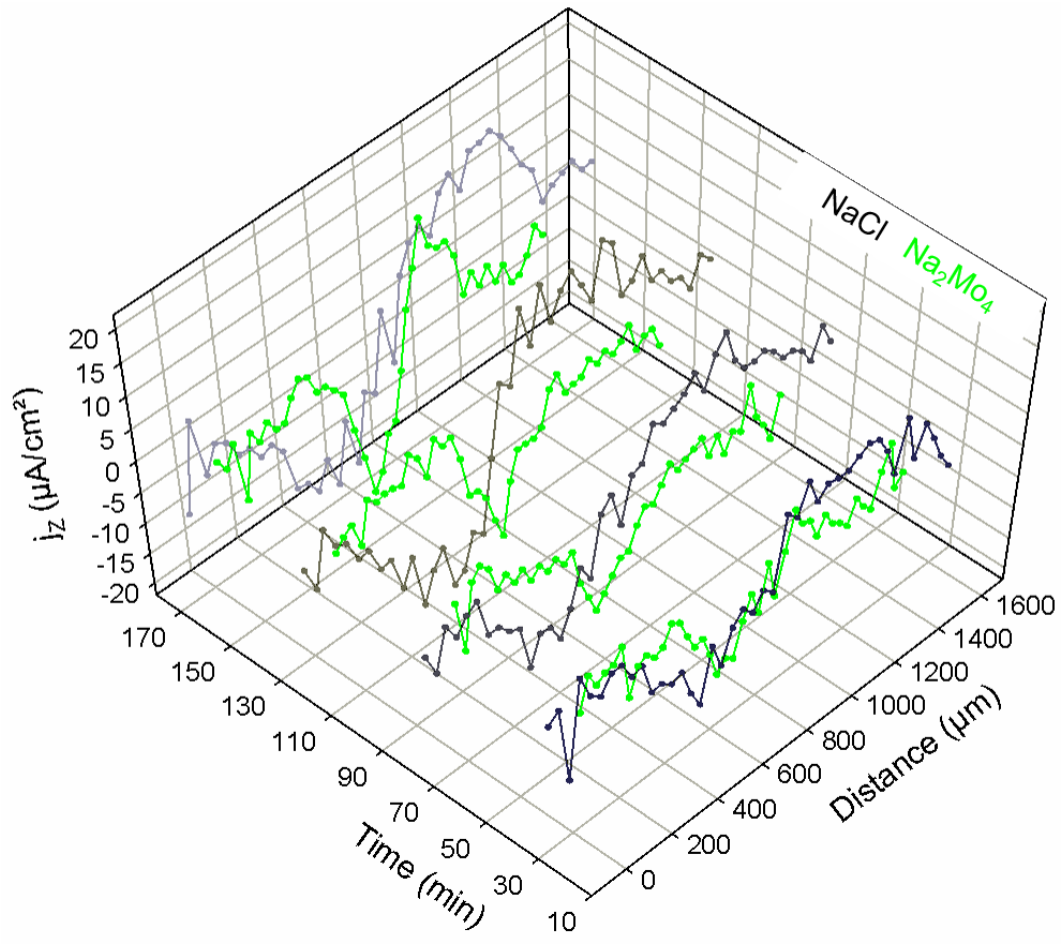

Fig. 14. j_Z line profiles constructed from the 4 consecutive SVET scans obtained in 0.05 M NaCl or 0.05 M NaCl + 5 mM Na_2MoO_4 during 180 min. The directions considered are indicated by lines r-r' (Fig. 10(b)) and i-i' (Fig. 13(b)) for the reference and the inhibitive solution, respectively.

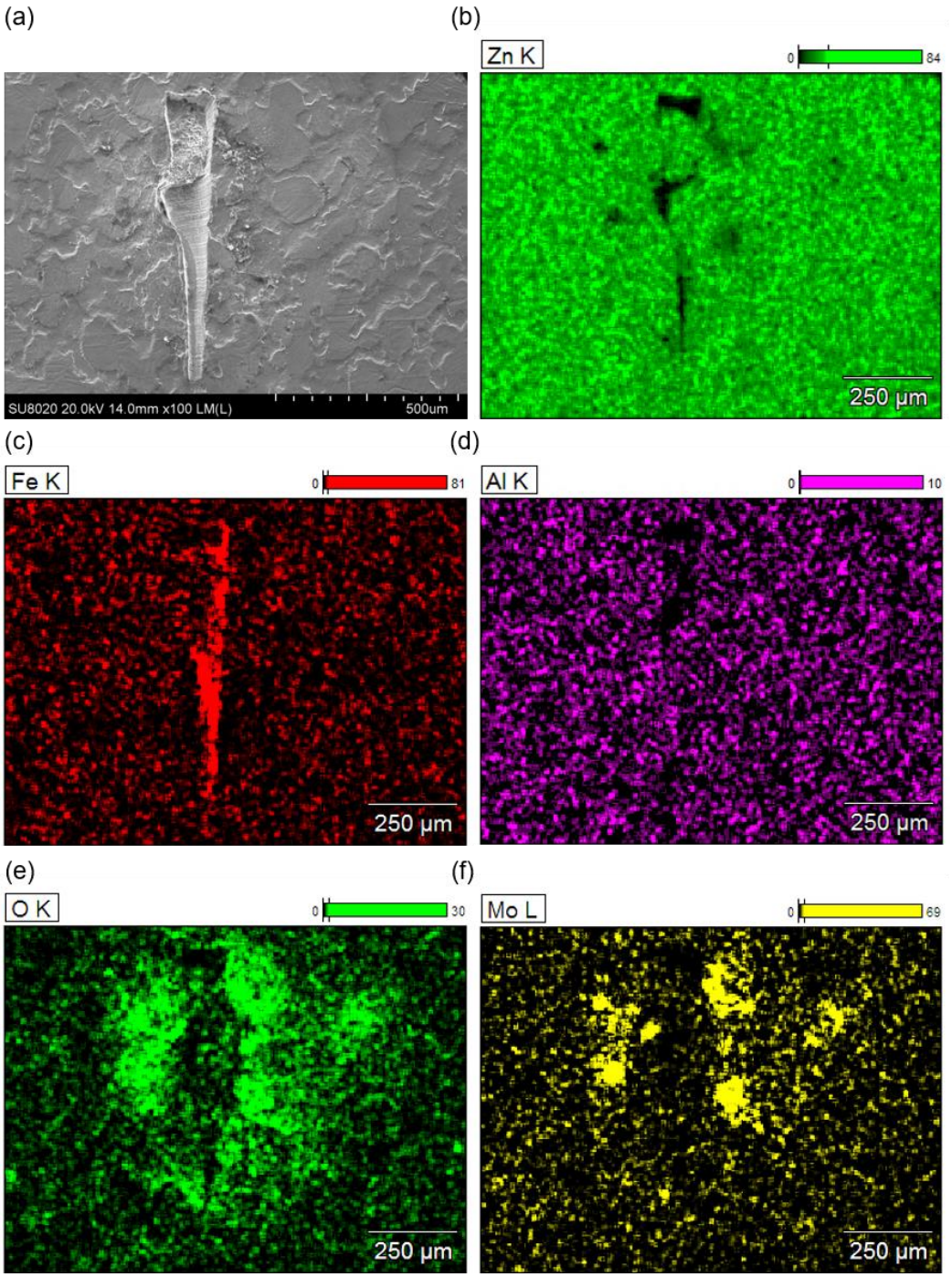

Fig. 15. SEM-EDX analysis of the severely scribed HDG surface after 180 min of immersion in 0.05 M NaCl + 5 mM Na_2MoO_4 electrolyte. (a) Secondary electron image. (b, c, d, e, f) Corresponding EDX elemental maps of Zn, Fe, Al, and O and Mo.

Highlights

- Na_2MoO_4 is tested as inhibitor on HDG/mild steel galvanic coupling model using ZRA
- Molybdate inhibits galvanic corrosion of skin-passed HDG/mild steel in 0.05 M NaCl
- SVET shows inhibition on skin-passed HDG mechanically scribed to the substrate
- The inhibitor changes corrosion mechanisms for both galvanic coupling conditions
- SVET shows corrosion behaviour of partially or completely scribed HDG Zn coatings

Graphical Abstract